# Intensity-Dependent Scattering Rings in High Order Above-Threshold Ionization

Baorui Yang,[1] K. J. Schafer,[2] B. Walker,[1] K. C. Kulander,[2,3] P. Agostini,[4] and L. F. DiMauro[1]
[1]*Chemistry Department, Brookhaven National Laboratory, Upton, New York 11973*
[2]*Lawrence Livermore National Laboratory, Livermore, California 94550*
[3]*Joint Institute for Laboratory Astrophysics, University of Colorado, Boulder, Colorado 80309*
[4]*Service de Recherches sur les Surfaces et l'Irradiation de la Matière, Centre d'Etudes Nucleáires de Saclay, 91191 Gif sur Yvette, France*
(Received 30 September 1993)

Angular distributions of high energy photoelectrons from Xe and Kr, excited by a 50 ps, 1.05 $\mu$m laser, are presented. In Xe, strong, narrow rings $\sim 45°$ off the polarization axis appear in a limited energy range centered around $9U_p$, where $U_p$ is the ponderomotive energy. This effect is much weaker in Kr. Single active electron calculations agree well with these observations. We conclude that the rings result from single-electron ionization dynamics, most likely involving rescattering from the ion core of the tunneling component of the continuum wave function.

PACS numbers: 32.80.Rm, 31.90.+s, 32.80.Fb

Much of our knowledge about strong field, multiphoton ionization processes comes from studies of the momentum characteristics of photoelectrons. In this regime electron energy distributions are observed to be a series of peaks separated by the photon energy [1] indicating the absorption of $S$ photons in excess of $N$, the minimum number required to overcome the field-free ionization potential. This process, called above-threshold ionization (ATI), is described at low intensities perturbatively as a one-step multiphoton transition between initial and continuum states. For a laser linearly polarized along the $z$ axis, the angular distributions (ADs) of the ejected electrons are expected to become more strongly peaked along this axis as $S$ increases, due to the propensity rule that favors increasingly higher angular momentum states as additional photons are absorbed. In the long wavelength, high intensity limit, ionization is dominated by the tunneling of electrons into the continuum during a short time around the peak of the electric field. Several authors have used a quasistatic model to describe this limit [2]. This model predicts that after the electron is freed from the atom, it is accelerated along the $z$ axis by the laser's electric field. The faster electrons are emitted before or after the peak of the field and are more likely to emerge close to the $z$ axis. Therefore we expect that the ADs become more elongated along the polarization axis as $S$ increases in both these limits. In this Letter we demonstrate that these simple pictures are incomplete.

We have measured the ADs of very high order ATI peaks (up to $S = 30$th order) from both xenon and krypton for laser intensities above $10^{13}$ W/cm$^2$. We observe unexpected structure in the ADs, which show the emission of high energy electrons at $\sim 45°$ off the $z$ axis. These electrons appear as pronounced side lobes on polar plots, or as "rings" in the full angular distribution due to the azimuthal symmetry about the $z$ axis. Their energies are surprisingly large, near $9U_p$, where $U_p$ is the intensity-dependent ponderomotive energy [3]. We have also calculated photoelectron ADs for xenon and krypton using the single active electron (SAE) approximation [4] to the time-dependent Schrödinger equation and find very good agreement with the measurements. The rings we find are clearly inconsistent with the simple behavior discussed above. Their existence and surprisingly strong intensity scaling challenge our understanding of the dynamics of strong field ionization.

From an experimental perspective, the detection and resolution of high order ATI electrons have been limited by a combination of space charge effects and low repetition rate laser sources ($\leq$ 10 Hz). Recently, we have increased our detection sensitivity by several orders of magnitude in dynamic range [5] by utilizing *kilohertz* repetition rate, gigawatt lasers. Consequently, it is now possible to explore the physics associated with very high order, strong-field processes while keeping the measurement time within reasonable limits.

Our experimental apparatus has been described in detail elsewhere [6]. We use a 1.05 $\mu$m, Nd:YLF laser system based on cw pumped regenerative amplification, which produces 4 mJ, 50 ps pulses at a repetition rate of $> 1$ kHz. The $TEM_{00}$ mode energy output is stable to $\pm$ 2% and has been well characterized [7]. The light is focused by $f/4$ optics into a UHV system which consists of an electron and mass time-of-flight spectrometer viewing the interaction region 180° apart. The acceptance angle of the electron spectrometer is $\sim 4°$. The electron ADs were collected by rotating the polarization direction of the laser relative to the space fixed spectrometer axis with a $\lambda/2$ waveplate. The $\lambda/2$ plate was optically characterized for phase distortions and the purity of the linear polarized light after the waveplate is measured to exceed 99%. The polar angle $\theta$ was varied over $> \pi$ radians to facilitate the detection of any asymmetries caused by imperfect alignment of the optics. Target pressures were maintained such that the count rate never exceeded 0.25 electron/shot (12–25 ions/shot), thus minimizing the effects of space charge. A data set (specific intensity or atom) was collected by randomizing the angular collec-


0031-9007/93/71(23)/3770(4)$06.00

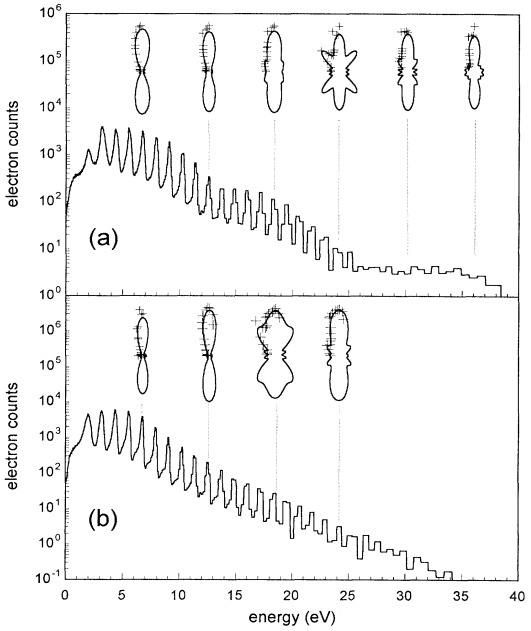


FIG. 1. The photoelectron energy spectrum of xenon with 50 ps, 1.05 $\mu$m excitation at (a) $3 \times 10^{13}$ W/cm$^2$ and (b) $1.9 \times 10^{13}$ W/cm$^2$. The spectra are an average of $7.2 \times 10^6$ laser shots. The insets are polar plots of the ADs for the $S = 5, 10, 15, \ldots$ ATI peaks. The solid line results from the Legendre fit and the raw data are shown as crosses.

tion sequence at fixed target density and normalization was achieved by referencing the 0° electron spectrum after every data point (angle). The reproducibility of each data set was checked in at least three independent runs.

Ionization of xenon into the $P_{3/2}$ continuum requires a minimum of $N = 11$, 1.05 $\mu$m photons, which produces an electron with $\sim 0.8$ eV kinetic energy. The energies of higher order peaks are given by $(S\hbar\omega + 0.8)$ eV, where $S = 1, 2, \ldots$ is the ATI order. In Fig. 1(a) we show a xenon electron energy spectrum recorded at the saturation intensity ($\sim 3 \times 10^{13}$ W/cm$^2$). The $S = 0$ and 1 peaks are suppressed due to ponderomotive channel closure [8], which provides an independent calibration of the laser intensity. The spectrum shows nicely resolved ATI out to the 21st order ($\sim 25$ eV). The electron peaks beyond 25 eV are instrumentally broadened but application of a retarding field reveals a resolvable series out to 40 eV. The dynamic counting range covers 7 orders of magnitude.

Also shown in Fig. 1(a) are representative ADs for different ATI orders ($S = 5, 10, 15, \ldots$). The data are fitted by a sum of even Legendre polynomials, $f(\theta) \equiv \sum_{\ell=0}^{n} \beta_{2\ell} P_{2\ell}(\cos\theta)$. The ADs for the first several peaks ($E \leq 15$ eV) are consistent with the expectations of our earlier discussion. The ionization is highly collimated along the $z$ axis with a slight narrowing with increasing $S$. However, as the order increases further the ADs for several peaks ($E > 15$ eV) exhibit unanticipated off-

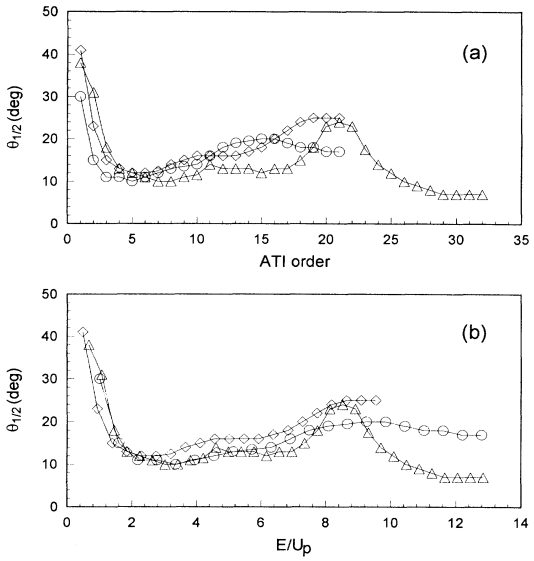


FIG. 2. Xenon half-angles as functions of (a) ATI order and (b) $E/U_p$, the electron energy over the ponderomotive energy, at 19 (circles), 25 (diamonds), and 30 (triangles) TW/cm$^2$. The value of $U_p$ used for each curve is defined by the laser's peak intensity.

axis structure (rings). For example, nearly one-half of the ionization signal in the $S = 20$ peak appears around 45° from the laser polarization axis [9]. Beyond these "structured" peaks the ADs of the highest ATI orders observed (e.g., $S = 25$ and 30) abruptly return to the strongly aligned shape. In Fig. 1(b), which is recorded at a lower intensity ($\sim 1.9 \times 10^{13}$ W/cm$^2$), the appearance energy of the rings has shifted to a lower ATI order (around $S = 15$). This energy shift is much larger than the corresponding 1.1 eV change in ponderomotive energy between these intensities. Although the detailed shapes of the rings and their directions of emission vary somewhat with intensity, their general appearance is relatively constant.

We find that the structured ADs always fall within a well defined, intensity-dependent energy window. The intensity dependence of this window is illustrated in Fig. 2(a). Here we show the half-angle of the polar distribution $\theta_{1/2}$, defined by

$$\frac{\int_0^{\theta_{1/2}} f(\theta) d\theta}{\int_0^{\pi/2} f(\theta) d\theta} = 0.5 \qquad (1)$$

for each ATI peak. There is a region of rapid narrowing in the ADs for the lowest-order ATI peaks ($S \leq 5$) due to the ponderomotive scattering of low energy electrons in the long pulse limit ($\tau_p \gg 1$ ps). This well known [8], intensity-dependent macroscopic field effect is negligibly small for the higher energy ADs. The presence of rings causes a large increase in $\theta_{1/2}$. It is clear the position and width of the peak in the half-angle distribution is

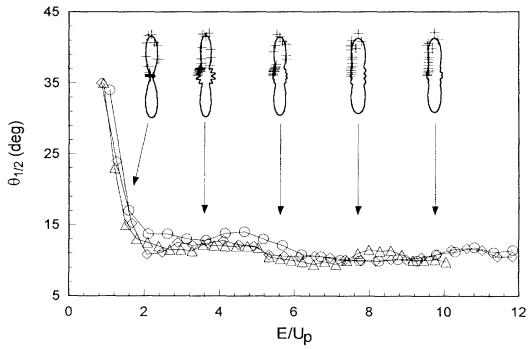


FIG. 3. Half-angles as functions of $E/U_p$ for krypton at intensities of 23 (circles), 29 (diamonds), and 40 (triangles) TW/cm$^2$. The insets are polar plots of the ADs for the $S = 5, 12, 19, 26, 33$ ATI peaks at 40 TW/cm$^2$.

strongly intensity dependent. As the laser intensity is increased the rings move rapidly to higher ATI orders.

A more revealing analysis of the intensity scaling is provided by plotting $\theta_{1/2}$ versus $E/U_p$, the electron energy scaled by the ponderomotive energy. Figure 2(b) shows the clear and dramatic "rephasing" of the peaks in the AD half-angles *within a narrow energy range centered around* $9U_p$. The $9U_p$ scaling signifies that the rings cannot be due simply to a mechanism associated with the $1U_p$ shift of the ionization threshold.

In Fig. 3 we present the half-angle distributions for krypton. The broadening associated with the rings found in xenon is conspicuously absent at all intensities studied. The plot shows only the initial ponderomotive narrowing referred to above, followed by an almost constant half-angle out to and beyond $10U_p$. The polar plots of representative ADs included as insets in Fig. 3 indicate some off-axis structure is present, but it is clearly much weaker in this atom.

We turn now to a discussion of possible physical explanations for the rings. We note that they appear on ATI peaks with energies large enough that either doubly excited states of the atom or excited states of the ion core could be involved. However, excited states of the ion core (which could conceivably play a role via resonant scattering) are expected to shift approximately ponderomotively, while doubly excited states should shift with intensity by at most $2U_p$, not the 8–$10U_p$ observed in the experiment. From this we conclude that the effect is due to single-electron ionization dynamics. In addition, the fact that the results for Xe and Kr differ indicates that atomic structure plays a crucial role in determining the degree of manifestation of this effect.

A relatively simple one-electron model that incorporates effects beyond both perturbation theory and the quasistatic tunneling picture is based upon the theory of Keldysh [10]. Ionization is described in this model as a one-step quantum transition from the initial ground state to a final (Volkov) state dressed by the laser field, neglecting any interaction with the ion core in the final state. Although it often underestimates the total ionization rate [11], it has shown some success in predicting low order ATI spectra [12]. ADs calculated in this model are known to show structure due to the interference of final state amplitudes. Using the experimental parameters and a xenon ground state constructed from a scaled hydrogenic $5p$ orbital, we calculated ATI spectra and ADs within this model for orders from 1 to 35 at various intensities. Though some features of the experiment are present, e.g., prominent lobes in the ADs for certain orders, there are many discrepancies: the overall shape of the ATI spectrum is wrong, dropping *much* too steeply at high energy; structures appear on isolated peaks, not a range of peaks and not at the energies seen in the experiment; and there is no scaling with intensity akin to the $9U_p$ scaling seen experimentally. Furthermore, the dependence upon the initial state (the only atomic parameter in the theory) can be expected to be very weak, in contrast to the dramatic difference between xenon and krypton illustrated in Figs. 1–3.

A more sophisticated model which contains all of the physics of the tunneling and Keldysh models and which can allow for the interaction of the electron with both the laser field and the ion core on an equal footing is the SAE approximation [4]. Within the SAE we determine the response of each valence electron to a laser pulse in the effective field of the remaining atomic electrons, frozen in their ground state orbitals. The SAE has been shown to provide accurate ionization rates, and in particular ATI spectra, for rare gases in the strong-field regime [5]. We have calculated the ADs for xenon and krypton at 1.05 $\mu$m and intensities $> 10^{13}$ W/cm$^2$ using this model. In the same manner as the experiments we calculate half-angles for the ADs. These are shown for xenon in Fig. 4 for three different intensities as a function of $E/U_p$. The qualitative behavior of the theoretical results is in excellent agreement with the experiments. In particular, the broadening of the ADs is confined to peaks near $9U_p$ [13]. We also include several polar plots of the ADs for xenon at the saturation intensity. The ADs show strong alignment along the $z$ axis except for a few orders near $9U_p$ which show large, narrow side lobes near $\sim 45°$. A similar calculation for krypton shows no well defined rings, only a weak broadening of the ADs near $9U_p$.

The appearance of the observed rings in the SAE calculations leads us to conclude that they are linked to the interaction of the ionizing electron with the ion core (as distinct from excitation of the core). Hence we refer to them as "scattering rings." Indeed, examination of the evolution of the time-dependent wave function reveals that electrons promoted to the continuum do interact strongly with the ion core before they leave the vicinity of the atom [14]. The experimental wavelength and intensities lie in a regime that is intermediate between multiphoton and tunneling ionization. We observe two

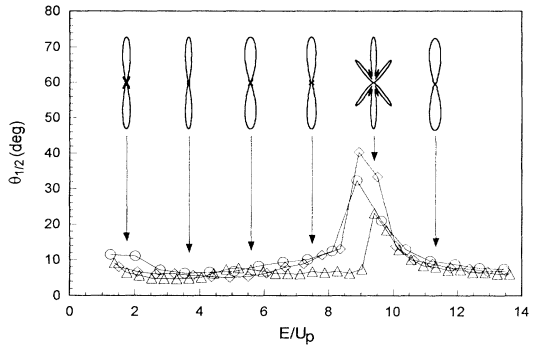


FIG. 4. Calculated Xe half-angles as functions of $E/U_p$ for 15 (circles), 20 (diamonds), and 30 (triangles) TW/cm$^2$. The insets are polar plots of the calculated ADs for the indicated ATI peaks at 30 TW/cm$^2$.

fairly distinct pieces to the ionizing wave function: one which acquires energy while still close to the ion core (as in a multiphoton transition), and another, representing the contribution from tunneling, which enters the continuum far from the nucleus during a short time around the peak of the electric field. Both can contribute to high order ATI via interaction with the ion core. Although there is no obvious reason why the rings cannot come from the multiphoton component, we observe that the rings remain prominent in the calculations as the intensity is increased (more tunneling) and are strongly suppressed when shorter wavelengths are used (less tunneling). We also find that in the experimental intensity range the tunneling portion of the krypton wave function is greatly reduced and broadened by comparison with xenon. The maximum drift energy of the tunneling component is limited within the quasiclassical model [2] to energies less than $3U_p$ in the long pulse limit. Additional drift energy [5] can only be gained when the tunneling wave packet returns to the ion core and rescatters. Simple classical estimates show that the resulting drift (cycle-averaged) energies can be as high as $11U_p$ if the electron is substantially backscattered. Because rescattering from the ion core depends sensitively on the short range part of the potential, it is not surprising that the shape and strength of the rings vary with atomic species. On the basis of the evidence we have presented, we conclude that the rings are caused by backscattering of the tunneling component of the ionizing wave function.

In summary, we have presented angular distributions for very high order ATI peaks that show unexpected off-axis stucture or "rings" at energies that scale as $\sim 9U_p$. We have identified these rings with the rescattering of electrons by the ion core during ionization. The high sensitivity of our measurment techniques has allowed us to study details of the ionization dynamics at much higher energies, on the scale of $U_p$, than any previously reported. Further experiments and calculations for other atomic systems are under way to more strongly establish this proposed mechanism.

We wish to thank D. Feldmann for access to his unpublished xenon results. We also acknowledge useful conversations with H. G. Muller, M. Lewenstein, and P. H. Bucksbaum. This research was carried out in part at Brookhaven National Laboratory under Contract No. DE-AC02-76CH00016 with the U.S. Department of Energy and supported by its Division of Chemical Sciences, Office of Basic Energy Sciences, and in part under the auspices of the U.S. Department of Energy at Lawrence Livermore National Laboratory under Contract No. W-7405-ENG-48. One of us (P.A.) acknowledges travel support from NATO Contract No. SA.5-2-05(RG910678).

[1] P. Agostini, F. Fabre, G. Mainfray, G. Petite, and N. K. Rahman, Phys. Rev. Lett. **42**, 1127 (1979).

[2] P. Corkum, N. Burnett, and F. Brunel, Phys. Rev. Lett. **62**, 1259 (1989); N. B. Delone and V. P. Krainov, J. Opt. Soc. Am. B **8**, 1207 (1991).

[3] The ponderomotive energy $U_p$ is defined in atomic units as $I/4\omega^2$, where $I$ and $\omega$ are the laser intensity and frequency, respectively. For 1.05 $\mu$m photons, $U_p = 1$ eV at $10^{13}$ W/cm$^2$.

[4] K. C. Kulander, K. J. Schafer, and J. L. Krause, Int. J. Quantum Chem. Symp. **25**, 415 (1991).

[5] K. J. Schafer, Baorui Yang, L. F. DiMauro, and K. C. Kulander, Phys. Rev. Lett. **70**, 1599 (1993).

[6] L. F. DiMauro, D. Kim, M. W. Courtney, and M. Anselment, Phys. Rev. A **38**, 2338 (1988).

[7] M. Saeed, D. Kim, and L. F. DiMauro, Appl. Opt. **29**, 1752 (1990).

[8] R. R. Freeman, P. H. Bucksbaum, and T. J. McIlrath, IEEE J. Quantum Electron. **24**, 1461 (1988).

[9] D. Feldmann (private communication). Similar electron "rings" were seen in some earlier unpublished work on xenon using a Nd:YAG multimode, nanosecond laser.

[10] L. V. Keldysh, Zh. Eksp. Teor. Fiz. **47**, 1945 (1964) [Sov. Phys. JETP **20**, 1307 (1964)]; F. H. M. Faisal, J. Phys. B **6**, L89 (1973); H. R. Reiss, Phys. Rev. A **22**, 1786 (1980).

[11] H. G. Muller, P. Agostini, and G. Petite, in *Atoms in Intense Laser Fields*, edited by M. Gavrila (Academic Press, Boston, MA, 1992).

[12] H. R. Reiss, J. Opt. Soc. Am. B **4**, 726 (1987).

[13] We have added $1U_p$ to the calculated electron energies to take account of the ponderomotive acceleration of the electrons present in these long pulse experiments.

[14] K. C. Kulander and K. J. Schafer, in *Proceedings of the International Conference on Multiphoton Processes VI*, edited by D. K. Evans (World Scientific, Singapore, 1993).